SIAM J. APPL. MATH.
Vol. 80, No. 2, pp. 906–928

TUMOR CONTROL, ELIMINATION, AND ESCAPE THROUGH A COMPARTMENTAL MODEL OF DENDRITIC CELL THERAPY FOR MELANOMA*

LAUREN R. DICKMAN†, EVAN MILLIKEN†, AND YANG KUANG†

Abstract. Melanoma, the deadliest form of skin cancer, is regularly treated by surgery in conjunction with a targeted therapy or immunotherapy. Dendritic cell therapy is an immunotherapy that capitalizes on the critical role dendritic cells play in shaping the immune response. We formulate a mathematical model employing ordinary differential and delay differential equations to understand the effectiveness of dendritic cell vaccines, accounting for cell trafficking with a blood and tumor compartment. We reduce our model to a system of ordinary differential equations. Both models are validated using experimental data from melanoma-induced mice. The simplicity of our reduced model allows for mathematical analysis and admits rich dynamics observed in a clinical setting, such as periodic solutions and bistability. We give thresholds for tumor elimination and existence. Bistability, in which the model outcomes are sensitive to the initial conditions, emphasizes a need for more aggressive treatment strategies, since the reproduction number below unity is no longer sufficient for elimination. A sensitivity analysis exhibits the parameters most significantly impacting the reproduction number, thereby suggesting the most efficacious treatments to use together with a dendritic cell vaccine.

Key words. Hopf bifurcation, backward bifurcation, dendritic cell therapy, partial rank correlation coefficient, stability analysis

AMS subject classifications. 68Q25, 68R10, 68U05

DOI. 10.1137/19M1276303

1. Introduction.

Skin cancer is the most common cancer diagnosis in the United States, with melanoma accounting for approximately 1% of all skin cancer [1]. Though a small percentage of the diagnoses, melanoma is the deadliest form of skin cancer and thus causes the majority of skin cancer–related deaths. Over the past 30 years, rapid increases have been seen in the incidences of melanoma [1]. The rise in melanoma has inspired additional research and advancements in its treatment.

Options for treatment consisted of excision, burning the tumor, amputation, and extirpation in the mid-to-late 19th century [2]. Eventually chemotherapy was introduced, though it did not result in improvements to the overall survival [3]. The introduction of chemotherapy represented a greater shift towards treating the internal cause of melanoma, as opposed to simply alleviating the associated pain. Treatment for melanoma now generally involves surgery followed by adjuvant therapies, often consisting of targeted therapy and immunotherapy. Targeted therapy uses drugs to target proteins, genes, and molecules which promote cancer growth, while immunotherapy works to enhance the immune system response against cancer, either through teaching it to react against something not previously considered foreign, like cancer cells, or releasing it to attack known antigens, as in the case of immune check-

*Received by the editors July 24, 2019; accepted for publication (in revised form) January 24, 2020; published electronically April 14, 2020.
https://doi.org/10.1137/19M1276303
Funding: This work was partially supported by the NIGMS of the National Institutes of Health (NIH) under award R01GM131405 and by the NSF under award DMS-1615879. The content is solely the responsibility of the authors and does not necessarily represent the official views of the NIH or the NSF.
†School of Mathematical and Statistical Sciences, Arizona State University, Tempe, AZ 85281 (lrjohns7@asu.edu, Evan.Milliken@asu.edu, kuang@asu.edu).

point inhibitors [4]. Compared to previous routine therapies, immunotherapy has shown great promise for melanoma patients [5].

Dendritic cells (DCs) originate in the bone marrow and are the most potent antigen-presenting cells (APCs) with a singular ability to initiate naive T cells [6]. As such, DC therapy has been employed to take advantage of the role DCs play in shaping the immune response. In this type of immunotherapy, immature DCs are extracted from the patient, cultured ex vivo, and loaded with tumor-associated antigens to become sensitized. Once sensitized and thereby activated, DCs are then injected back into the patient, where they migrate to the lymphoid organs via the bloodstream. Within the lymphoid organs, the activated (mature) DCs interact with the naive cytotoxic T lymphocytes (CTLs), activating them and instructing them to proliferate. These activated CTLs, otherwise known as effector cells, travel to the tumor, where they mount a fight against cells expressing the tumor-associated antigen. The cancer cells and the immunosuppressive environment of the tumor are able to inactivate CTLs or induce CTL apoptosis, and the activated CTLs in turn kill the tumor cells [7]. The immune system retains a memory response to these formerly encountered antigens through the existence of memory CTLs, leading to the long-term impacts of immunotherapies.

Human clinical trials involving DC-based vaccines commenced in the 1990s, yielding positive results for patients with melanoma [8], prostate cancer [9], and B-cell lymphoma [10]. Over 400 clinical trials evaluating DC vaccines are currently being carried out in the United States, of which 237 are Phase II and 11 are Phase III [11]. Since the beginnings of DC-based vaccine-related clinical trials, a number of malignancies have been tested with the immunotherapy, including intracranial tumors [12], multiple myeloma [13], renal cell carcinoma [14], colorectal cancer [15], and cervical cancer [16]. Furthermore, various treatment strategies, including prophylactic (pre-exposure) dosing, have been studied. Prolonged survival and limited side effects have been observed in patients with a vast array of tumor types treated with DC-based vaccines [13]. Prophylactic dosing with DC-based vaccines, useful for patients with a high risk of developing cancer, has been observed to effectively inhibit certain types of cancers when studied in vivo [17]. However, the most effective use of the DC vaccine has been shown with combination treatments. The low toxicity of the DC vaccine greatly adds to its appeal as part of a combination therapy and, as such, DC vaccines are often tested in conjunction with other treatments, such as chemotherapy, immune checkpoint inhibitors, and radiotherapy [18]. Mathematical models allow for a deeper look into the behavior of the vaccine and an exploration into what mechanisms lead to treatment success or failure during these clinical trials, consequently motivating and informing new clinical trials. Once a greater understanding of the monotherapy is established, clear extensions would involve incorporating combination treatments to better comprehend the synergy. Additional insights into these key mechanisms decidedly prove valuable when designing combination therapies.

Immunotherapy treatments, particularly DC vaccines, have been a recent focus of mathematical modeling efforts. Within the last 15 years, a number of researchers have examined optimal DC treatment protocols by studying systems of ordinary differential equations (ODEs) through the lens of various optimal control strategies [19, 20, 4, 21, 22]. Furthermore, ODEs have been employed recently in working towards the goal of precision medicine. Gevertz and Wares [23] sought to find a simpler form of an ODE model that would better allow for personalization of the parameters and individualized fitting, while still maintaining the ability to describe the data and key biological features for cancer treatment of DC injections and viruses engineered to infect and

kill cancer cells. Additionally, models exploring DC therapy for melanoma have tested differing dosing strategies using delay differential equations (DDEs) [24, 25, 26]. In hopes of using in silico tests to reduce the economic burden of searching for and experimenting with new protocols, Castillo-Montiel et al. [24] studied the question of how to improve the efficacy of DC treatment through simulating various treatment strategies and evaluating the sensitivity to changes in parameters.

In studying the effects of DC injections in mice, Ludewig et al. [26] developed a delay differential compartment model representing DC and CTL trafficking. De Pillis, Gallegos, and Radunskaya [25] proposed a modification and extension of Ludewig et al.'s model, most notably by the addition of a tumor compartment. The de Pillis–Gallegos–Radunskaya model of nine DDEs and ODEs consisted of DCs in the blood, tumor, and spleen, activated CTLs in the blood, tumor, and spleen, memory CTLs in the blood and spleen, and tumor cells. Murine melanoma data from Lee, Cho, and Lee [27] was used in calibrating model parameters. Simulations of tumor growth were validated against the data and then explored through various dosing strategies. They concluded that even with the most aggressive dosing regimen, regardless of whether an intratumoral or intravenous injection, DC treatment could not completely eradicate the tumor after the tumor had already presented itself. However, if DC treatment was administered before the tumor challenge, with the fractional tumor kill rate by CTLs sufficiently large, the tumor was able to be eradicated. Due to the complexity of the model, they were limited in their ability to do mathematical analysis.

DC therapy seeks to eradicate tumor cells by exciting a tailored immune response. The de Pillis–Gallegos–Radunskaya model captures the dynamics of immune system excitement in the spleen compartment and the dynamics of eradication in the tumor compartment. The blood compartment captures transport between the other two. In this article, the de Pillis–Gallegos–Radunskaya model is reduced in two stages. By introducing delay, we collapse the blood and spleen into a single compartment, while still accounting for the time it takes for DCs and activated CTLs to travel through the body. The tumor compartment is retained. Thus, the dynamics of excitement and eradication are still accounted for. By making several biological assumptions, including quasi–steady state assumptions for certain cell populations and simplified functional response for cell-cell interactions, the model is further reduced to a system of four nonlinear ODEs. Since the utility of the model is for assessing treatment in a short period of time, the assumptions can be deemed reasonable. Both the intermediate (including delay) and the reduced models are justified using clinical data from melanoma-induced mice. The reduced model is simple enough to allow for mathematical analysis. That analysis reveals complicated dynamics, including bistability and periodic solutions. In addition to describing the data, the reduced model captures clinically observed phenomena, such as oscillatory tumor-immune behavior. Several numerical experiments, particularly bifurcation diagrams, bistability tests for various initial tumor sizes, examinations of eigenvalues as parameters change, limit cycle simulations, partial rank correlation coefficient (PRCC) sensitivity analyses, and tumor responses to various dosing strategies, are provided to verify the results of the mathematical analysis and to test treatment strategies.

The article is organized as follows. A thorough description of the process of model reduction is provided in section 2. The mathematical analysis of the reduced model is provided in sections 3, 4, and 5. Sensitivity analysis and additional numerical experiments are included in section 6. The main results are summarized and discussed in section 7.

2. Model formulation. Our model is based on de Pillis, Gallegos, and Radunskaya's model [25] with several main modifications. De Pillis, Gallegos, and Radunskaya's model captures the interactions between DCs, activated and memory CTLs, and tumor cells in spleen, blood, and tumor compartments. DC therapy consists of injecting activated DC cells intravenously or intratumorally. DCs then travel through the blood to the spleen, where they stimulate the activation of CTLs, which in turn travel through the blood back to the tumor to eradicate tumor cells. In the de Pillis–Gallegos–Radunskaya model, the blood is a means of transport for dendritic cells and effector cells between the spleen and the tumor. The primary focus of their work involved examining optimal hypothetical DC treatments. From the perspective of the tumor, the treatment has the net effect of changing the flow of DCs and active CTLs into the tumor. Since we are chiefly interested in the effectiveness of the therapy, it is reasonable to model some of the interactions away from the tumor compartment implicitly, rather than explicitly. To that end, we introduce a delay to account for the history of the DCs and CTLs as they travel through the blood to the spleen. This allows us to model the activation of naive and memory CTLs in the blood, while implicitly accounting for the fact that activation actually takes place in the spleen. Our first reduced model (intermediate model) of six DDEs and ODEs captures the movement between two compartments: the blood and the tumor. The model consists of DCs in the blood (D_b), DCs in the tumor (D_t), tumor cells (T), memory CTLs in the blood (E_b^m), activated CTLs in the blood (E_b^a), and activated CTLs in the tumor (E_t^a), all of which are represented by the circles in Figure 1. We additionally incorporate the effect of competition for space within the tumor compartment by adding negative feedback on the tumor cell growth from activated CTLs and DCs, as also shown in Figure 1.

The other major change is the choice of functional response for the interactions between CTLs and DCs. The de Pillis–Gallegos–Radunskaya model assumes naive cells are activated at a constant rate when DCs are present. To reflect the biology of the cell-cell interactions better, we instead allow Michaelis–Menten kinetics to govern the interaction between naive CTLs and DCs. Finally, we assume a constant influx of activated CTLs from the spleen to the blood. We refer to the resulting model as the intermediate model. Figure 1 provides a diagram of the intermediate model.

The intermediate model is given by the following system:

$$\frac{dD_b}{dt} = \underbrace{v_b(t)}_{\text{injection}} + \underbrace{\mu_{TB}D_t}_{\text{migration}} - \underbrace{\mu_{BT}D_b\frac{T}{K_T+T}}_{\text{tumor recruitment}} - \underbrace{\delta_D D_b}_{\text{death}}, \tag{2.1a}$$

$$\frac{dD_t}{dt} = \underbrace{v_t(t)}_{\text{injection}} + \underbrace{D_i\frac{T}{K_T+T}}_{\text{activation}} + \underbrace{\mu_{BT}D_b\frac{T}{K_T+T}}_{\text{tumor recruitment}} - \underbrace{\mu_{TB}D_t}_{\text{migration}} - \underbrace{\delta_D D_t}_{\text{death}}, \tag{2.1b}$$

$$\begin{aligned}\frac{dE_b^a}{dt} = {} & \underbrace{s_{E^a}}_{\text{source}} + \underbrace{e^{-\delta_{E^a}\tau}\frac{D_b(t-\tau)E_n}{\theta_n+D_b(t-\tau)}}_{\text{activation/proliferation}} + \underbrace{b_m e^{-\delta_{E^a}\tau}\frac{D_b(t-\tau)E_b^m(t-\tau)}{\theta_m+D_b(t-\tau)}}_{\text{activation/proliferation}} \\ & - \underbrace{r_{am}E_b^a}_{\text{becoming memory}} - \underbrace{\mu_{BTE}E_b^a\frac{T}{K_T+T}}_{\text{migration}} - \underbrace{\delta_{E^a}E_b^a}_{\text{death}},\end{aligned} \tag{2.1c}$$

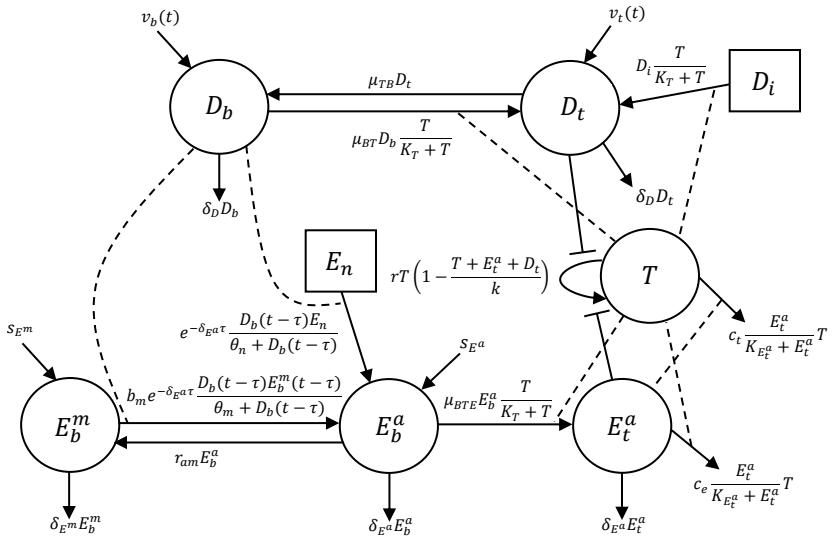

FIG. 1. *The interactions governing* (2.1). *Dashed lines represent a catalytic effect, flat-headed arrows represent an inhibitory effect, and straight arrows connecting populations represent movement between populations, whether through entering a new compartment or becoming activated/inactivated. The circles represent the variables of the system, while squares represent cell populations per day assumed to be constant.* $D_b, D_t, E_b^m, E_b^a, E_t^a, T, E_n$, *and* D_i *represent DCs in the blood, DCs in the tumor, memory CTLs in the blood, activated CTLs in the blood, activated CTLs in the tumor, tumor cells, the number of naive CTLs activated/proliferating per day, and the number of immature DCs being activated per day. The* μ *parameters represent maximum transfer rates between compartments,* δ *parameters reflect death of the cell populations, and* s *parameters act as source terms. Intratumoral and intravenous DC injections are given by* $v_t(t)$ *and* $v_b(t)$, *respectively.* r, k, c_t, c_e, b_m, *and* r_{am} *reflect the tumor cell growth rate, tumor cell carrying capacity, maximum rate activated CTLs kill the tumor cells, maximum rate tumor cells inactivate CTLs, maximum activation/proliferation rate of memory CTLs by DCs, and natural inactivation rate of activated CTLs. All parameter values and descriptions are listed in Table* SM1 *in the supplementary materials.*

$$\text{(2.1d)}\qquad \frac{dE_t^a}{dt} = \underbrace{\mu_{BTE}E_b^a\frac{T}{K_T+T}}_{\text{migration}} - \underbrace{c_e\frac{E_t^a}{K_{E_t^a}+E_t^a}T}_{\text{inactivation by tumor}} - \underbrace{\delta_{E^a}E_t^a}_{\text{death}},$$

$$\text{(2.1e)}\qquad \frac{dE_b^m}{dt} = \underbrace{s_{E^m}}_{\text{source}} \underbrace{- b_m e^{-\delta_{E^a}\tau}\frac{D_b(t-\tau)E_b^m(t-\tau)}{\theta_m+D_b(t-\tau)}}_{\text{activation/proliferation}} + \underbrace{r_{am}E_b^a}_{\text{becoming memory}} - \underbrace{\delta_{E^m}E_b^m}_{\text{death}},$$

$$\text{(2.1f)}\qquad \frac{dT}{dt} = \underbrace{rT\left(1-\frac{T+E_t^a+D_t}{k}\right)}_{\text{growth}} - \underbrace{c_t\frac{E_t^a}{K_{E_t^a}+E_t^a}T}_{\text{death by CTL}}.$$

A description of the model parameters and their values for fitting, along with the related sources from the literature, are given in Table SM1 in the supplementary materials, linked from the main article webpage. The parameters unable to be found in the literature were fixed using melanoma data from Lee, Cho, and Lee [27].

The behavior of the DCs moving between the blood and tumor compartments is captured through (2.1a) and (2.1b), respectively. The functions $v_b(t)$ and $v_t(t)$ are

source terms modeling intravenous and intratumoral DC injections. As functions of time, these source terms allow for numerical testing of dosing strategies. DC transfer from the blood to the tumor occurs at a maximum rate of μ_{BT}, with the population of tumor cells catalyzing the movement. Once the DCs are sensitized and loaded with tumor antigens, they leave the tumor to migrate towards the lymphoid organs via the blood at a maximum rate of μ_{TB} to interact with the CTLs. A daily number of immature DCs, D_i, become sensitized and activated as they interact with the tumor cells. Following standard practice as in [28], the model assumes Michaelis–Menten kinetics in all immune and tumor-immune interactions. The Michaelis–Menten kinetics allow for a representation of saturated immune responses and can also capture the effects of only portions of the tumor being able to interact with the immune cells at a time.

The activated CTLs migrate between the blood and tumor compartments as given by (2.1c) and (2.1d). The prolonged interaction between DCs and CTLs required for activation and the time accounting for their travel from the lymphoid organs are represented by a delay in interactions between memory and naive CTLs and DCs. Through these interactions with the DCs, the naive and memory CTLs are instructed to multiply at maximum rates b_n and b_m, respectively. Following an absence of contact with the tumor-associated antigen, activated CTLs in the blood return to a resting memory state at rate r_{am} [29]. We assume a constant influx s_{E^a} of activated CTLs from the spleen to the blood. The presence of the tumor helps to catalyze the migration of the activated CTLs from the blood to the tumor at a maximum rate of μ_{BTE}. Once in the tumor, the activated CTLs interact with the tumor, becoming inactivated by the tumor cells at a rate of c_e.

Equation (2.1e) governs the dynamics of the memory CTLs in the blood. We assume a constant influx s_{E^m} of memory CTLs from the spleen to the blood. Additionally, the activation of memory CTLs acts as a loss, and inactivation of E_b^a acts as a source term.

The first term of the right-hand side of (2.1f) accounts for tumor growth. In a variety of models, tumor growth has been modeled with a logistic [25, 30], exponential [31], power law [32], or Gompertzian [24, 33] approach. We assume competition for space from the activated CTLs and DCs in the tumor compartment negatively impacts the tumor growth. The activated CTLs kill the tumor cells at rate c_t. By using Michaelis–Menten kinetics to govern the killing of the tumor cells, we are able to capture the effects of melanoma being a solid tumor, where immune cells can only contact fractions of the tumor at a time.

To determine the validity of our biological assumptions and simplifications, we compare our model to the de Pillis–Gallegos–Radunskaya model [25] using clinical data given in Lee, Cho, and Lee [27]. The mouse experiments in Lee, Cho, and Lee [27] examine the tumor volume with and without DC treatment. All mice were injected with 5×10^5 B16F10 cells to induce malignant melanomas. Intratumoral doses ranging from 0 to 21×10^5 DCs were administered 6, 8, and 10 days following the B16F10 cell inoculation. In computing tumor volume, we assume tumor cells are spherical. We approximate the diameters to be 20 μm, in accordance with the mean B16F10 cell diameter recorded in recent measurements [34].

From Figure 2a, we observe that our intermediate model can closely reproduce the experimentally observed tumor reductions from various doses of DCs. While fitting data does not necessarily validate mathematical models, the ability of our model to describe clinical data does help justify incorporating our additional biological details and simplifications. Additionally, we note that even though the intermediate model

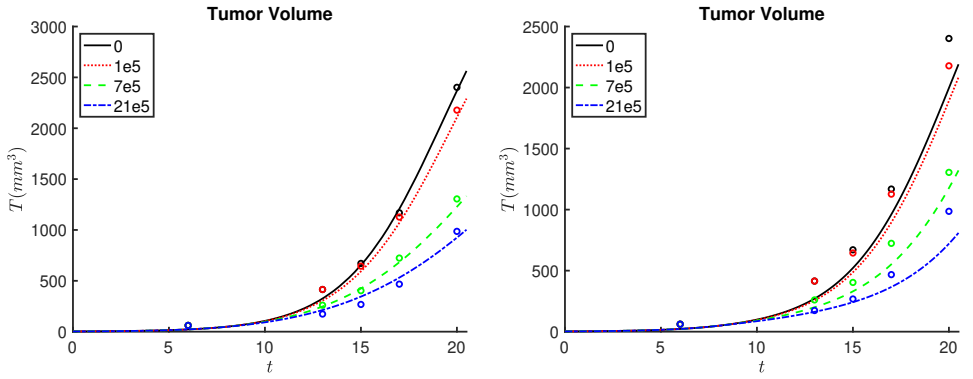

(a) Intermediate model (2.1) (b) de Pillis–Gallegos–Radunskaya model [25]

FIG. 2. *The fit to the data from Lee, Cho, and Lee* [27] *with* (a) *the intermediate DDE and ODE model* (2.1) *and* (b) *the de Pillis–Gallegos–Radunskaya model* [25]. *Mean relative errors for the fits are given in Table* 2.

is simpler than the de Pillis–Gallegos–Radunskaya model, it is comparable in terms of fitting, as outlined in Table 2 and demonstrated in Figure 2.

Having formulated the intermediate model, we go on to make several simplifying assumptions supported by biological observations. Through studying a variety of species, including both mice [35] and humans [36, 37], the memory T cells have been found to turn over faster than the naive T cells. We assume that this turnover is happening rapidly such that the memory CTLs are at a quasi–steady state. Additionally, since the model is only intended to assess treatment for a short period of time, we can reasonably assume the DC movement between the blood and tumor compartments is independent of the tumor size during the brief period being considered. We simplify the representation of cell-cell interactions by supposing mass action kinetics, as opposed to Michaelis–Menten kinetics. We assume that the proportion of activated CTLs in the tumor, $\frac{E_t^a}{E_t^a+E_b^a}$, is approximately constant. This constant ratio allows us to combine (2.1c) and (2.1d) into a single equation for the effector cells, given by (2.2c). These assumptions lead to further model reductions and the formulation of the reduced model (2.2), which is analytically tractable.

TABLE 1
Variables of the simplified model (in cells).

Variable	Description
D_b	DCs in the blood
D_t	DCs in the tumor
E	activated CTLs
T	tumor cells

The variables of the simplified model, their meanings, and their units are listed in Table 1. Parameter values are outlined in Table SM2 in the supplementary materials. The simplified system takes the following form:

$$\frac{dD_b}{dt} = v_b(t) - \mu_{BT} D_b + \mu_{TB} D_t - \delta_D D_b, \tag{2.2a}$$

$$\frac{dD_t}{dt} = v_t(t) + D_i T + \mu_{BT} D_b - \mu_{TB} D_t - \delta_D D_t, \tag{2.2b}$$

$$\frac{dE}{dt} = s_E + cD_b - c_e ET - (r_{am} + \delta_E)E, \tag{2.2c}$$

$$\frac{dT}{dt} = rT\left(1 - \frac{T + E + D_t}{k}\right) - c_t ET. \tag{2.2d}$$

The assumptions that lead to the reduced model are further justified by a fit to clinical data, as displayed in Figure 3.

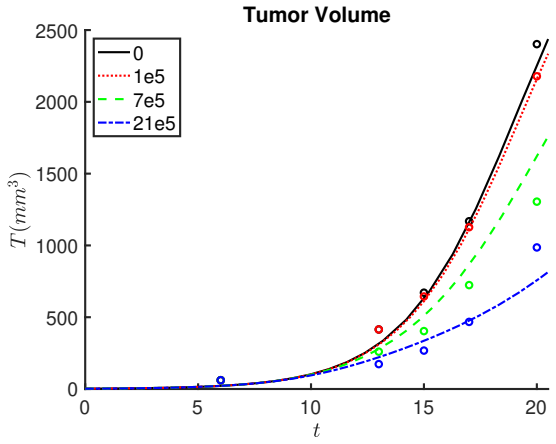

FIG. 3. *The fit to the data from Lee, Cho, and Lee* [27] *with the simplified ODE model* (2.2). *The mean relative error for the fit is given in Table* 2.

Despite the reductions made, the model remains able to describe the data from all four trials with a single set of fixed, biologically reasonable parameters. As the simplified model is comparable in terms of fitting to both the de Pillis–Gallegos–Radunskaya model and the intermediate model, as outlined in Table 2 and Figures 2 and 3, it is worth mathematically studying to extract insights, since the complexity of the other models allows for far less analysis.

TABLE 2
Mean relative errors for various model formulations.

Model	Mean relative error
System (2.1): intermediate model (DDE and ODE)	0.204766
System (2.2): simplified model (ODE)	0.230647
de Pillis–Gallegos–Radunskaya model [25]	0.291335

3. Preliminary analysis. The analysis that follows is based on the reduced model given by system (2.2). In this section, we establish basic results of the model, like well-posedness, dissipativity, and the existence of equilibria. In addition, we determine the basic reproduction number $\mathcal{R}_0$. Unless otherwise stated, we assume that all of the parameters of (2.2) are positive.

PROPOSITION 3.1. *Suppose that* $v_b(t)$ *and* $v_t(t)$ *are smooth, bounded functions of* t. *Then system* (2.2) *is well-posed and point dissipative.*

Proof. Let $x = (D_b, D_t, E, T)$, and let ϕ_t be the flow of (2.2). Writing (2.2) as the vector equation $x = f(t, x)$, since $v_b(t)$ and $v_t(t)$ are smooth, we have that f is continuously differentiable and $x = f(t, x)$ is well-posed. By examining the flow on the boundary, we see that for $i = 1, 2, 3$, if $x_i = 0$, then $(\phi_t(x))_i > 0$ for $t > 0$. The subspace $\{x \in \mathbb{R}^4 | T = 0\}$ is fully invariant. By the previous arguments, the restriction of this fully invariant to its intersection with the nonnegative orthant is forward invariant. By Grönwall's inequality, if $x_4 > 0$, then $(\phi_t(x))_4 > 0$.

It follows that $\dot{T} \leq rT(1 - \frac{T}{k})$. Given $T(0) \geq 0$, given $\varepsilon > 0$, there exists t_0 such that $T(t) < k + \varepsilon$ for all $t > t_0$. Since v_b and v_t are bounded, there exist positive constants C_1 and C_2 such that if $D = D_b + D_t$, then $\dot{D} < A - BD$ for $t > t_0$. It follows that given $\varepsilon > 0$, there exists $t_1 > t_0$ such that $D(t) = D_b(t) + D_t(t) < \frac{C_1}{C_2} + \varepsilon$ for all $t > t_1$. Taken together, there exist positive constants C_3 and C_4 such that $\dot{E} < C_3 - C_4 E$ for $t > t_1$. Given $\varepsilon > 0$, there exists $t_2 > t_1$ such that $E(t) < \frac{C_3}{C_4} + \varepsilon$ for all $t > t_2$. Fix $\varepsilon > 0$, and let $C_5 = \max(k, \frac{C_1}{C_2}, \frac{C_3}{C_4}) + \varepsilon$. For any nonnegative initial condition x, there exists $t_2 > 0$ such that $\phi_{t+t_2}(x) \in [0, C_5]^4$ for all $t > 0$. Thus, system (2.2) is point dissipative. ∎

For the purpose of simplifying the mathematical analysis, we make the assumption that $v_b(t) = v_b$ and $v_t(t) = v_t$ are constant and nonnegative. The next result is the existence and uniqueness of a tumor-free equilibrium.

PROPOSITION 3.2. *System* (2.2) *admits the unique tumor-free equilibrium* $E_0 = (D_{b*}, D_{t*}, E_*, 0)$.

Proof. Suppose $T = 0$; then $\dot{T} = 0$, and (2.2a) and (2.2b) decouple from (2.2) to form the planar cooperative system

$$\begin{aligned} \dot{D}_b &= v_b - \delta_D D_b - \mu_{BT} D_b + \mu_{TB} D_t, \\ \dot{D}_t &= v_t - \delta_D D_t + \mu_{BT} D_b - \mu_{TB} D_t, \end{aligned} \tag{3.1}$$

which admits the unique equilibrium (D_{b*}, D_{t*}) given by

$$D_{b*} = \frac{\mu_{TB} v_t + (\delta_D + \mu_{TB}) v_b}{\delta_D(\delta_D + \mu_{BT} + \mu_{TB})}, \quad D_{t*} = \frac{(\delta_D + \mu_{BT}) v_t + \mu_{BT} v_b}{\delta_D(\delta_D + \mu_{BT} + \mu_{TB})}.$$

Substituting $T = 0$ and $D_b = D_{b*}$ into (2.2c) yields

$$E_* = \frac{s_e + c D_{b*}}{\widetilde{\delta}_E}.$$ ∎

The treatment we are considering involves tailoring the immune system to launch an enhanced response targeting tumor cells. From the perspective of the immune system in this context, tumor cells can be viewed as similar to an infectious disease. We borrow the notion of the basic reproduction number from the study of infectious disease dynamics. The basic reproduction number, denoted by $\mathcal{R}_0$, is defined as the average number of secondary infections generated by a single infectious individual in a totally susceptible population during the lifetime of the infectious individual. In the present context, the basic reproduction number can be viewed as a ratio of the proliferation potential of a tumor cell to the strength of a combination of the immune response and crowding effects. The basic reproduction number can be calculated using the next generation matrix approach [38, 39].

PROPOSITION 3.3. *The basic reproduction number $\mathcal{R}_0$ is given by*

$$\mathcal{R}_0 = \frac{k}{\left(1+\frac{kc_t}{r}\right)E_* + D_{t*}}. \tag{3.2}$$

Proof. Note that $\dot{T} = \mathcal{F}(D_b, D_t, E, T) - \mathcal{V}(D_b, D_t, E, T)$, where $\mathcal{F}$ represents the new infections (tumor cells) and $\mathcal{V}$ represents the rate of tumor cells leaving the system. We can then decouple (2.2d) from the rest of (2.2) when close to the disease-free equilibrium, E_0. Thus, $\frac{dT}{dt} = (F-V)T$. We then have

$$F = \left(\frac{\partial \mathcal{F}}{\partial T}\right)\bigg|_{E_0} = r, \qquad V = \left(\frac{\partial \mathcal{V}}{\partial T}\right)\bigg|_{E_0} = \frac{r}{k}(E_* + D_{t*}) + c_t E_*.$$

Now the next generation operator $FV^{-1} = \frac{k}{\left(1+\frac{kc_t}{r}\right)E_* + D_{t*}}$. Therefore,

$$\mathcal{R}_0 = \frac{k}{\left(1+\frac{kc_t}{r}\right)E_* + D_{t*}}, \tag{3.3}$$

where E_* and D_{t*} correspond to the steady states of the activated CTLs and DCs in the tumor when the system is tumor-free. ∎

Remark 3.4. Suppose that r is the dominant eigenvalue of the Jacobian of (2.2) evaluated at E_0. Then r and $\mathcal{R}_0 - 1$ have the same sign. In models of infectious disease dynamics, it is common that the disease-free equilibrium undergoes a transcritical bifurcation as $\mathcal{R}_0$ increases through the critical value $\mathcal{R}_0 = 1$ resulting in the emergence of a unique positive equilibrium. However, system (2.2) produces more complicated dynamics. While it is indeed the case that (2.2) admits a unique positive equilibrium when $\mathcal{R}_0 > 1$, it may admit two positive equilibria when $\mathcal{R}_0 < 1$. We will see that the existence of these two positive equilibria is the result of a backward bifurcation in section 4.

PROPOSITION 3.5. *If $\mathcal{R}_0 \geq 1$, then there exists a unique positive equilibrium, E_1. For k sufficiently large, there exist constants C_6 and $\mathcal{R}_{crit}$ such that if $c_e > C_6$ and $\mathcal{R}_{crit} < \mathcal{R}_0 < 1$, then in addition to E_1, there exists an additional positive equilibrium, E_2.*

Proof. Suppose $T^* > 0$. From (2.2a),

$$D_b^* = \frac{\mu_{TB}}{\delta_D + \mu_{BT}} D_t^* + \frac{v_b}{\delta_D + \mu_{BT}}. \tag{3.4}$$

From $\dot{D}_t = 0$, we have

$$D_t^* = \frac{D_i(\delta_D + \mu_{BT})}{\delta_D(\delta_D + \mu_{BT} + \mu_{TB})} T^* + \frac{v_t(\delta_D + \mu_{BT}) + v_b\mu_{BT}}{\delta_D(\delta_D + \mu_{BT} + \mu_{TB})} = c_4 T^* + D_{t*}. \tag{3.5}$$

Combining (3.4) and (3.5) yields

$$D_b^* = \frac{D_i\mu_{TB}}{\delta_D(\delta_D + \mu_{BT} + \mu_{TB})} T^* + \frac{v_t\mu_{TB} + v_b(\delta_D + \mu_{TB})}{\delta_D(\delta_D + \mu_{BT} + \mu_{TB})} = c_3 T^* + D_{b*}. \tag{3.6}$$

From $\dot{T} = 0$, $T^* = 0$ or

$$E^* = -\frac{(1+c_4)}{1+\frac{kc_t}{r}} T^* + \frac{k - D_{t*}}{1+\frac{kc_t}{r}}. \tag{3.7}$$

Recall that for $T(0) > 0$, after finite time we have $0 < T < k+\varepsilon$. Therefore, $(\dot{D}_b, \dot{D}_t)^T$ is greater than the monotone planar system (3.1). It follows that $D_b^* > D_{b*} - \varepsilon$ in finite time. Therefore, after finite time, $\dot{E} > s_E + cD_{b*} - (\widetilde{\delta}_E + k)E$. Thus, we must have that $E^* > 0$.

Substituting (3.6) and (3.7) into $\dot{E} = 0$ yields $g(T) = \mathcal{A}_0 T^2 + \mathcal{A}_1 T + \mathcal{A}_2 = 0$, where

$$\mathcal{A}_0 = \frac{c_e(1+c_4)}{1+\frac{kc_t}{r}}, \tag{3.8a}$$

$$\mathcal{A}_1 = cc_3 + \frac{\widetilde{\delta}_E(1+c_4)}{1+\frac{kc_t}{r}} - \frac{c_e(k-D_{t*})}{1+\frac{kc_t}{r}}, \tag{3.8b}$$

$$\mathcal{A}_2 = \frac{\widetilde{\delta}_E}{1+\frac{kc_t}{r}}\left[\left(1+\frac{kc_t}{r}\right)\frac{s_E+cD_{b*}}{\widetilde{\delta}_E} + D_{t*} - k\right]. \tag{3.8c}$$

Note that $\operatorname{sgn}(\mathcal{A}_2) = \operatorname{sgn}(1-\mathcal{R}_0)$. If $\mathcal{R}_0 > 1$, then $\mathcal{A}_2 < 0$ and $g(T)$ is a concave up parabola with $g(0) < 0$. Therefore, there exists a unique positive solution, T_1^*, of $g(T) = 0$ when $\mathcal{R}_0 > 1$. In light of (3.6), (3.5), and (3.7), $E_1 = (D_b^*(T_1^*), D_t^*(T_1), E^*(T_1^*), T_1^*)$ is the unique positive equilibrium of (2.2) when $\mathcal{R}_0 > 1$.

Now, $\mathcal{R}_0$ is monotonically decreasing in s_E with $\lim_{s_E\to\infty}\mathcal{R}_0 = 0$. Rewriting $\mathcal{A}_2 = s_E + cD_{b*} - \widetilde{\delta}_E\frac{k-D_{t*}}{1+\frac{kc_t}{r}}$, it is clear that $\lim_{s_E\to\infty}\mathcal{A}_2 = +\infty$. Suppose that initially $\mathcal{R}_0 > 1$, as in the previous case. We increase s_E until $\mathcal{R}_0 = 1$. Then $\mathcal{A}_2 = 0$ and $g(T^*)$ has two real roots, $T^* = 0$ and $T^* = \frac{-\mathcal{A}_1}{\mathcal{A}_0}$. If

$$c_e > C_6 = \frac{1+\frac{kc_t}{r}}{k-D_{t*}}\left(\widetilde{\delta}_E\frac{1+c_4}{1+\frac{kc_t}{r}} + cc_3\right), \tag{3.9}$$

then $\mathcal{A}_1 < 0$ and $T^* = \frac{-\mathcal{A}_1}{\mathcal{A}_0} > 0$. By continuity, there exists $\delta > 0$ such that $g(T^*)$ has two real distinct positive roots for $1-\delta < \mathcal{R}_0 < 1$. Now consider the discriminant, $\mathscr{D} = \mathcal{A}_1^2 - 4\mathcal{A}_0\mathcal{A}_2$, of g. If $\mathcal{R}_0 = 1$, then $\mathscr{D} = \mathcal{A}_1^2 > 0$. Since $\mathcal{A}_2$ monotonically increases from zero as we decrease $\mathcal{R}_0$ (say by increasing s_E), there exists a unique s_1 such that if $s_E = s_1$, then $\mathcal{A}_2 = \frac{\mathcal{A}_1^2}{4\mathcal{A}_0}$, which implies that $\mathscr{D} = 0$. Let

$$\mathcal{R}_{crit} = \frac{k}{(1+\frac{kc_t}{r})\frac{s_1+cD_{b*}}{\widetilde{\delta}_E} + D_{t*}}. \tag{3.10}$$

It follows that if $c_e > C_6$, then $g(T^*)$ has two positive roots $T_1^* > T_2^*$ for $\mathcal{R}_{crit} < \mathcal{R}_0 < 1$. Setting $E_i = (D_b^*(T_i^*), D_t^*(T_i), E^*(T_i^*), T_i^*)$ for $i = 1, 2$, the result follows. ∎

The next two results are related to the stability of the tumor-free equilibrium, E_0. It was noted in the proof of Proposition 3.1 that the subspace $\{(D_b, D_t, E, T) \in \mathbb{R}^4 | T = 0\}$ is fully invariant. Let X_2 be the intersection of this fully invariant subspace with the nonnegative orthant. From examination of the flow on the boundary, it follows that X_2 is forward invariant. The following result deals with the stability of the tumor-free equilibria in X_2. At first glance, this result may appear to lack biological relevance. However, it is critical ground work for later results regarding the existence or eradication of the tumor.

PROPOSITION 3.6. *The tumor-free equilibrium is globally asymptotically stable* (G.A.S.) *in the forward invariant boundary subspace* X_2.

Proof. As noted in the proof of Proposition 3.2, when $T = 0$, (2.2a) and (2.2b) decouple from system (2.2) to form the monotone planar system (3.1) which admits the equilibrium (D_{b*}, D_{t*}). Let $D = D_b + D_t$. Then $\dot{D} = \dot{D}_b + \dot{D}_t = v - \delta_D D$, where $v = v_b + v_t$. Thus, for any $D(0) \geq 0$,

$$\lim_{t\to\infty} D(t) = \lim_{t\to\infty} D_b(t) + D_t(t) = \frac{v}{\delta_D}.$$

It follows from application of Theorem 2.2 of Smith [40] that solutions of (3.1) with nonnegative initial conditions converge to (D_{b*}, D_{t*}). Therefore, for any $\epsilon > 0$, solutions of (3.1) with nonnegative initial conditions enter $\{(D_b, D_t) : |D_b - D_{b*}| < \epsilon\}$ in finite time.

The remaining equation describing the flow in X_2 is given by

$$\dot{E} = s_E + cD_b - \widetilde{\delta}_E E,$$

where $\widetilde{\delta}_E = r_{am} + \delta_E$. For any $\epsilon > 0$, for any initial data in X_2, after finite time,

$$s_E + c(D_{b*} - \epsilon) - \widetilde{\delta}_E E < \dot{E} < s_E + c(D_{b*} + \epsilon) - \widetilde{\delta}_E E.$$

The result follows by the comparison principle. ∎

Next, we consider the stability of E_0 in the full space $\bar{\mathbb{R}}^4_+$. At this stage, we are limited to local stability analysis.

PROPOSITION 3.7. *$E_0 = (D_{b*}, D_{t*}, E_*, 0)$ is locally asymptotically stable when $\mathcal{R}_0 < 1$ and unstable when $\mathcal{R}_0 > 1$.*

Proof. The Jacobian of system (2.2) evaluated at the tumor-free equilibrium E_0 is given by

$$\mathbf{J}|_{E_0} = \begin{pmatrix} -\mu_{BT} - \delta_D & \mu_{TB} & 0 & 0 \\ \mu_{BT} & -\mu_{TB} - \delta_D & 0 & D_i \\ c & 0 & -\widetilde{\delta}_E & -c_e E_* \\ 0 & 0 & 0 & r\left(1 - \frac{1}{\mathcal{R}_0}\right) \end{pmatrix}, \tag{3.11}$$

which admits eigenvalues

$$\lambda_1 = r\left(1 - \frac{1}{\mathcal{R}_0}\right); \lambda_2 = -\widetilde{\delta}_E; \lambda_3 = -\delta_D; \lambda_4 = -(\delta_D + \mu_{TB} + \mu_{BT}).$$

Thus, E_0 is locally asymptotically stable when $\mathcal{R}_0 < 1$, and E_0 is unstable when $\mathcal{R}_0 > 1$. ∎

4. Backward bifurcation and bistability. In this section, we return attention to the possibility of the existence of two positive equilibria described in Proposition 3.5. In Remark 3.4, we allude to the fact that, in epidemiological models, it is typical for a disease-free equilibrium to undergo a transcritical bifurcation with a unique positive equilibrium as $\mathcal{R}_0$ increases through the critical value of 1. Another possibility is that of a backward bifurcation. Backward bifurcations in epidemiological models have been associated with modeling assumptions that lead to loops among infected and susceptible classes as a result of reinfection or waning immunity, for example. Our next result is a proof of the existence of a backward bifurcation in system (2.2),

via analysis of the center manifold and Theorem 4.1 of [41]. Interestingly, this backward bifurcation relies on the rate that activated CTLs are inactivated as a result of interacting with tumor cells. One feature of backward bifurcations in epidemiological models is that they can generally be eliminated by assuming mass action, rather than frequency-dependent functional response. Similar to a tuberculosis model outlined in [42], it is possible to exhibit backward bifurcation in models with mass action functional response, and system (2.2) is an example of that.

Rearranging (3.3), it follows that

$$\operatorname{sgn}(\mathcal{R}_0 - 1) = \operatorname{sgn}\left(k - \frac{E_* + D_{t*}}{1 - \frac{c_t}{r}E_*}\right).$$

It is always possible to make $1 - \frac{c_t}{r}E_* > 0$, by making c_t sufficiently small. That is, if

$$c_t < C_7 = \frac{r}{E_*}, \tag{4.1}$$

then there exists unique $k^* > 0$ such that $k = k^*$ implies that $\mathcal{R}_0 = 1$.

THEOREM 4.1. *If $\mathcal{R}_0 = 1$ and $c_t < C_7$, then there exists $C_8 > 0$ such that system (2.2) undergoes a backward bifurcation at E_0 as c_e increases through C_8.*

Proof. We first recall that the Jacobian, J, of (2.2) evaluated at the disease-free equilibrium, E_0, is given by (3.11), where $j_{44} = r\left(1 - \frac{1}{\mathcal{R}_0}\right)$ is the only nonzero entry in the fourth row. Since $c_t < C_7$, there exists $!k^* > 0$ such that $k = k^*$ implies $\mathcal{R}_0 = 1$. Setting $k = k^*$, we have that zero is a simple eigenvalue of J, and all other eigenvalues have negative real part. Hence, we apply center manifold theory to analyze the dynamics near $k = k^*$. The right eigenvector of J associated with the eigenvalue 0 is given by

$$w = \left[c_3, c_4, \frac{cc_3 - c_eE_*}{\underset{\sim}{\delta}_E}, 1\right]^T,$$

where c_3 and c_4 are given in (3.6) and (3.5), respectively. The left eigenvector associated with the eigenvalue 0 is given by

$$v = [0, 0, 0, 1].$$

Rewrite (2.2) as $\dot{x} = f(x, \psi)$, where x and $f(x, \psi)$ are vectors in $\mathbb{R}^4$ and $\psi = k$. Following Castillo-Chavez and Song [41], we compute the following sums:

$$a = \sum_{k,i,j=1}^{n} v_k w_i w_j \frac{\partial^2 f_k}{\partial x_i \partial x_j}(E_0, k^*), \qquad b = \sum_{k,i=1}^{n} v_k w_i \frac{\partial^2 f_k}{\partial x_i \partial \psi}(E_0, k^*).$$

Since $v = [0, 0, 0, 1]$, we need only consider the partial derivatives of $f_4(x)$. Direct calculation reveals that

$$a = -2\frac{r}{k}(c_4 + 1) - 2\left(\frac{r}{k} + c_t\right)\left(\frac{cc_3 - c_eE_*}{\underset{\sim}{\delta}_E}\right),$$

$$b = \frac{r(E_* + D_{t*})}{k^2}.$$

Then b is always positive and $a > 0$ if and only if

$$c_e > C_8 = \frac{1}{E_*}\left(\widetilde{\delta}_E\left(\frac{1+c_4}{1+\frac{c_t k}{r}}\right) + cc_3\right). \tag{4.2}$$

The statement follows from application of Theorem 4.1 in Castillo-Chavez and Song [41]. ∎

This backward bifurcation consists of two codimension-one bifurcations, a saddle node bifurcation together with a transcritical bifurcation. By tuning the vertex of the degree 2 polynomial for T^*, we can reduce the region of bistability associated with the backward bifurcation and even eliminate it by making the saddle node and transcritical bifurcation points coincide. In this case, we have a pitchfork-like bifurcation. We may further perturb the vertex into the infeasible region, $T^* < 0$, where bistability exists in a mathematical sense but has no biological meaning. The critical value where the two bifurcation points collide and result in a pitchfork-like bifurcation corresponds to making $\mathcal{A}_1 = 0$. From (3.8b), $\mathcal{A}_1 = 0$ if and only if

$$cc_3 + \frac{\widetilde{\delta}_E(1+c_4)}{1+\frac{kc_t}{r}} - \frac{c_e(k-D_{t*})}{1+\frac{kc_t}{r}} = 0,$$

which, when $\mathcal{R}_0 = 1$, is equivalent to

$$cc_3 + \frac{\widetilde{\delta}_E(1+c_4)}{1+\frac{kc_t}{r}} - c_e E_* = 0 \iff a = 0.$$

Figure 4 illustrates the cases where $a > 0$, $a = 0$, and $a < 0$.

The stability of the various branches of equilibria is determined by Theorem 4.1 in [41]. Since

$$\frac{k-D_{t*}}{1+\frac{kc_t}{r}} = \frac{\left(\left(1+\frac{kc_t}{r}\right)E_* + D_{t*}\right)\mathcal{R}_0 - D_{t*}}{1+\frac{kc_t}{r}},$$

we may view C_6 as a decreasing function of $\mathcal{R}_0$ with $C_6|_{\mathcal{R}_0=1} = C_8$ and $C_6 > C_8$ when $\mathcal{R}_0 < 1$. Then $\mathcal{R}_0 = \mathcal{R}_{crit}$ corresponds to the saddle node bifurcation point and $\mathcal{R}_0 = 1$ corresponds to the transcritical bifurcation point. Together this results in the following corollary. Figure 5 illustrates the bistability indicated in the corollary.

COROLLARY 4.2. *Suppose the assumptions of Theorem* 4.1 *hold. Then system* (2.2) *exhibits bistability for* $\mathcal{R}_{crit} < \mathcal{R}_0 < 1$.

The next result describes the conditions for the global stability of the tumor-free equilibrium. We only consider the case in which the system exhibits a backward bifurcation and a pair of positive equilibria for $\mathcal{R}_{crit} < \mathcal{R}_0 < 1$.

THEOREM 4.3. *Suppose that the conditions of Theorem* 4.1 *hold. Then there exists* $C_9 > 0$ *such that if* $\mathcal{R}_0 < C_9$, *then the tumor-free equilibrium is G.A.S.*

Proof. By hypothesis, Corollary 4.2 implies that system (2.2) admits two distinct positive equilibria for $\mathcal{R}_{crit} < \mathcal{R}_0 < 1$. By construction, the choice of s_1 used to formulate $\mathcal{R}_{crit}$ in (3.10) guarantees that when $\mathcal{R}_0 = \mathcal{R}_{crit}$, the discriminant $\mathscr{D} = \mathcal{A}_1^2 - 4\mathcal{A}_0\mathcal{A}_2 = 0$. Thus, if $\mathcal{R}_0 < \mathcal{R}_{crit}$, or equivalently $s_E > s_1$, then E_0 is the only equilibrium of (2.2). We will proceed using comparison arguments. To that end, it is necessary to assume that

$$s_E > s_2 = \left(\widetilde{\delta}_E + c_e k\right)\frac{k-D_{t*}}{1+\frac{kc_t}{r}} - cD_{b*}. \tag{4.3}$$

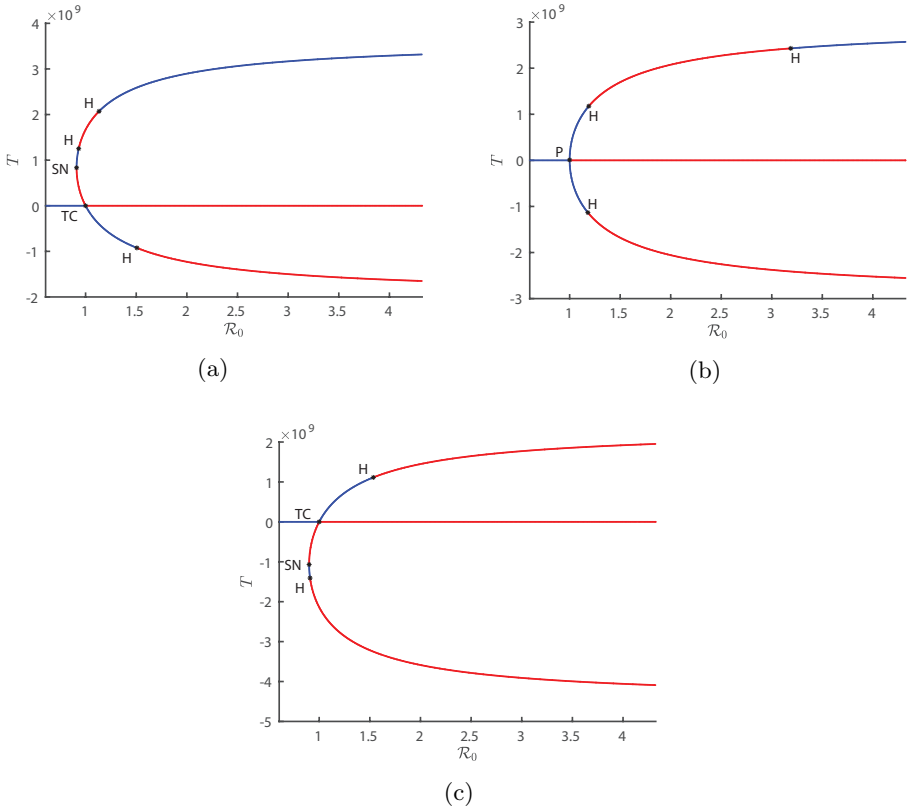

FIG. 4. *Backward bifurcation* (a)*, pitchfork-like bifurcation* (b)*, and transcritical bifurcation* (c) *of the tumor-free equilibrium* E_0*, with H: Hopf bifurcation, SN: saddle-node bifurcation, TC: transcritical bifurcation, and P: pitchfork-like bifurcation. The blue lines represent stable equilibria, while the red lines represent unstable equilibria.*

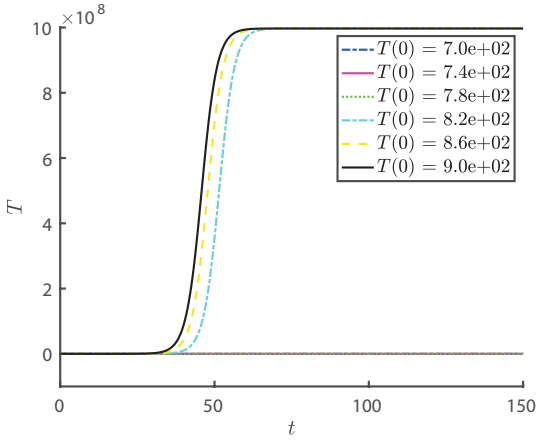

FIG. 5. *Bistability exhibited as initial tumor burden increases with a fixed* $v_b = 6.2 \times 10^3$*. We take* $v_t = 0$*,* $\mu_{BT} = 9.826 \times 10^{-9}$*,* $\mu_{TB} = 0.0011$*,* $\delta_D = 0.34$*,* $D_i = 0.001$*,* $s_E = 0.1$*,* $c = 3.205$*,* $c_e = 10^{-4}$*,* $r_{am} = 0.01$*,* $\delta_E = 0.1155$*,* $r = 0.3994$*,* $k = 10^9$*,* $c_t = 3.5 \times 10^{-6}$*, satisfying the condition* (4.2) *needed for a backward bifurcation.*

Let $s_E^* = \max(s_1, s_2)$:

$$C_9 = \frac{k}{(1+\frac{kc_t}{r})\frac{s_E^*+cD_{b*}}{\widetilde{\delta}_E} + D_{t*}}. \tag{4.4}$$

Now consider the flow of (2.2) when $T(0) > 0$. From (2.2d), $\dot{T} < rT\left(1-\frac{T}{k}\right)$. Therefore, for any $\varepsilon > 0$, there exists $t_0 > 0$ such that $T(t) < k + \varepsilon$ for all $t > t_0$. Similarly, (2.2a) and (2.2b) are greater than or equal to the planar system (3.1) so that for any $\varepsilon > 0$, there exists $t_1 > t_0$ such that $D_b(t) > D_{b*} - \varepsilon$ and $D_t(t) > D_{t*} - \varepsilon$ for all $t > t_1$. It follows that, for any $\varepsilon > 0$, for $t > t_1$,

$$\dot{E} > s_E + c(D_{b*} - \varepsilon) - E(\widetilde{\delta}_E + c_e(k+\varepsilon)).$$

For $\varepsilon > 0$, the equilibrium of the linear equation on the right-hand side of the inequality is

$$\frac{s_e + c(D_{b*} - \varepsilon)}{\widetilde{\delta}_E + c_e(k+\varepsilon)}.$$

Thus, for $\varepsilon > 0$, there exists $t_2 > t_1$ such that

$$E(t) > \frac{s_E + cD_{b*}}{\widetilde{\delta}_E + c_e k} - \varepsilon$$

for all $t > t_2$.

Since $\mathcal{R}_0 < C_9$, we have $s_E > s_E^*$ and $\frac{(1+\frac{kc_t}{r})\frac{s_E+cD_{b*}}{\widetilde{\delta}_E+c_ek}+D_{t*}}{k} > 1$. Fix

$$\varepsilon_1 = \frac{1}{2}\left[\frac{(1+\frac{kc_t}{r})\frac{s_E+cD_{b*}}{\widetilde{\delta}_E+c_ek}+D_{t*}}{2+\frac{kc_t}{r}} - \frac{k}{2+\frac{kc_t}{r}}\right].$$

Then, for $t > t_2$,

$$\dot{T} < rT\left(1 - \frac{T + (1+\frac{kc_t}{r})\left[\frac{s_E+cD_{b*}}{\widetilde{\delta}_E+c_ek} - \varepsilon_1\right] + D_{t*} - \varepsilon_1}{k}\right) < 0.$$

For $t > t_2$, $T(t)$ is decreasing and bounded below. Thus, $\lim_{t\to\infty} T(t) = \alpha < \infty$. By Barbalat's lemma, $\lim_{t\to\infty} \dot{T} = 0$. Since $s_E > s_E^* \geq s_1$, the only possibility is $\alpha = 0$. The omega limit set of the initial point x_0 with $T(0) > 0$ contains a point in the forward invariant boundary set, X_2, described in the comments preceding Proposition 3.6. By Proposition 3.6, the omega limit set of any point in X_2 is the singleton $\{E_0\}$, so $\{E_0\} \subset \omega(x_0)$. If $\omega(x_0)$ contains a point other than E_0, then it would have to have $T > 0$, since E_0 is G.A.S in X_2. However, this is a contradiction of the fact that $\lim_{t\to\infty} T(t) = 0$. Thus, $\omega(x_0) = \{E_0\}$. ∎

Remark 4.4. By the definition of s_E^*, we have $C_9 \leq \mathcal{R}_{crit}$, with equality when $s_1 \geq s_2$. Conditions for the positivity of $(s_1 - s_2)$ have proven elusive. The difficulty is in the requirement that $c_e > C_6$, since C_6 depends on all of the remaining parameters, either directly or through dependence on c_3 and c_4. In the case that $s_1 < s_2$, we have $C_9 < \mathcal{R}_{crit}$, suggesting that perhaps $\mathcal{R}_{crit}$ is not a sharp threshold. However, numerical experiments suggest the stability of E_0 for $\mathcal{R}_0 < \mathcal{R}_{crit}$ even when $s_1 < s_2$. It remains an open question as to how to close the gap between C_9 and $\mathcal{R}_{crit}$ in the case that $s_1 < s_2$.

It has been found clinically that response rates for DC vaccines are two to three times higher in the adjuvant setting when compared to the metastatic setting [43]. In an adjuvant setting, the tumor burden is already lessened by previous treatments. Additionally, it has been observed that DCs are insufficient as a monotherapy in treating advanced melanoma, yielding $< 10\%$ improvements in objective response rates. This behavior corresponds qualitatively to what might be expected in the bistable region described above.

5. Hopf bifurcation and periodic solutions. In addition to a backward bifurcation, numerical experiments indicate the existence of Hopf bifurcations leading to periodic solutions to system (2.2). First, fix our choice of parameters. If we view $\mathcal{R}_0$ as a function of r, then it is an increasing function of r, since

$$\frac{d}{dr}\mathcal{R}_0(r) = \frac{k^2 c_t E_*}{((r + kc_t)E_* + D_{t*})^2} > 0.$$

Next, we numerically compute the eigenvalues of the Jacobian evaluated at E_1. We do this as we vary r from 0.005 to 7 by increments of 1×10^{-3}. Plotting the eigenvalues in the complex plane, we see that a complex conjugate pair crosses from the left half-plane to the right half-plane at approximately $r = 0.233$. This indicates a supercritical Hopf, which we can detect via numerical integration of (2.2). The same conjugate pair of eigenvalues cross back at approximately $r = 6.806$. Thus, the periodic orbit either disappears, or there is a second subcritical Hopf. The plot of the eigenvalues as we vary r is presented in Figure 6. An analytical proof of the Hopf bifurcation remains an open question.

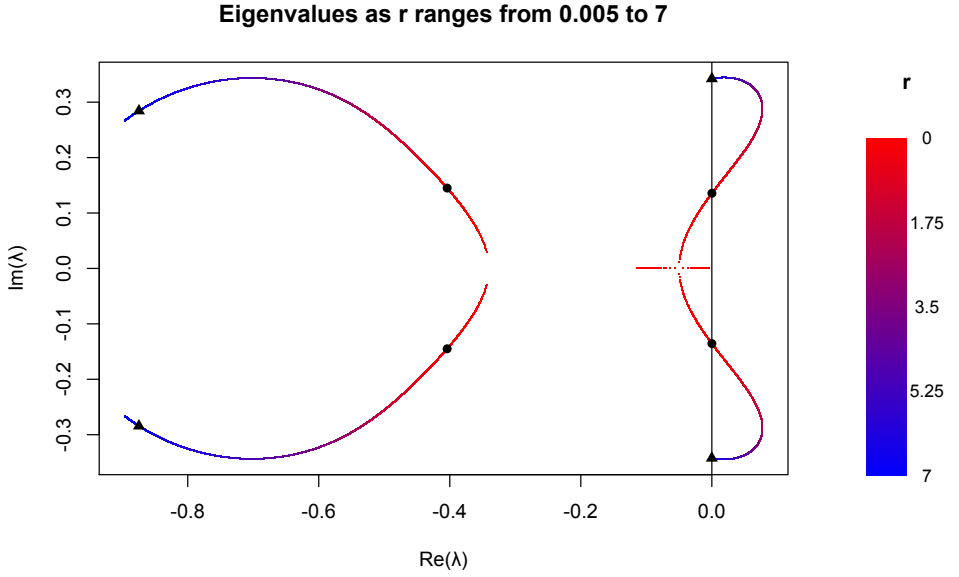

FIG. 6. *Eigenvalues of the Jacobian of* (2.2) *evaluated at* E_1 *as* r *varies from* 0.005 *to* 7 *in increments of* 0.001 *with* $v_b = 0$, $v_t = 0$, $\mu_{BT} = 1.272 \times 10^{-5}$, $\mu_{TB} = 0.0011$, $\delta_D = 0.34$, $D_i = 0.00126$, $s_E = 0.01189$, $c = 0.127$, $c_e = 9.42 \times 10^{-14}$, $\widetilde{\delta}_E = 0.1255$, $k = 10^9$, $c_t = 0.0035$.

Remark 5.1 (Bogdanov–Takens bifurcation). Recall the pitchfork-like bifurcation illustrated in Figure 4. The bifurcation on the branch equilibria with $T < 0$ is

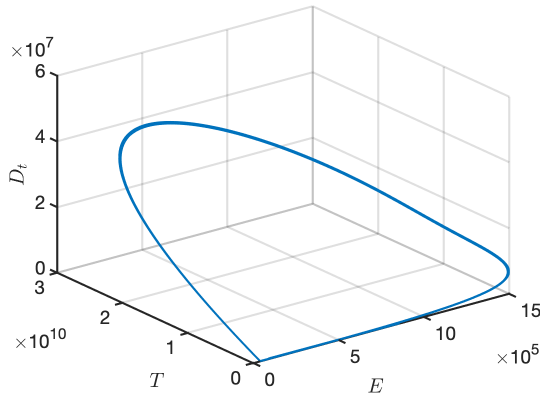

FIG. 7. *Projection of limit cycle in* $\mathbb{R}^3$ *when* $v_b = 0$, $v_t = 0$, $\mu_{BT} = 9.826 \times 10^{-9}$, $\mu_{TB} = 0.0011$, $\delta_D = 0.34$, $D_i = 0.001$, $s_E = 5 \times 10^3$, $c = 3.205$, $c_e = 9.42 \times 10^{-14}$, $r_{am} = 0.01$, $\delta_E = 0.1155$, $r = 0.9$, $k = 5 \times 10^{12}$, 3.5×10^{-6}. *Simulations run for* $t = 2000$ *days.*

a Hopf bifurcation. The close proximity of a pitchfork-like bifurcation and Hopf bifurcation in the parameter space suggests the possibility of a Bogdanov–Takens (BT) bifurcation. Since we insist that all parameters other than v_b and v_t are strictly positive, the Jacobian evaluated at E_0, given in (3.11), can have at most a single zero eigenvalue. However, if we let $\widetilde{\delta}_E = 0$, J admits a double zero eigenvalue. In the case of a BT, the magnitude of periodic orbits around equilibria on the positive and negative branches increases until the birth of homoclinic connections from the equilibrium at $T = 0$. Then a periodic orbit appears which contains all three equilibria in its interior (in normal form with interior in the sense of a Jordan curve; cf. [44, p. 329]). However, in our system, the equilibrium with $T = 0$ is in the fully invariant set $\{(D_b, D_t, E, T) \in \mathbb{R}^4 | T = 0\}$. Therefore, once homoclinic orbits appear, they persist even as the magnitude of oscillations continues to increase. Some numerical experiments, as in Figure 7, suggest the presence of a homoclinic connection from E_0 to itself as the magnitude of oscillatory solutions increases. In order to study the BT, we must consider the limit as $\widetilde{\delta}_E \to 0$. However, $\lim_{\widetilde{\delta}_E \to 0} E_* = \infty$. It may be possible to make a change of variables ($\frac{1}{E_*} \to 0$ as $\widetilde{\delta}_E \to 0$). A full analysis of a possible BT bifurcation is beyond the scope of this article.

6. Numerical analysis.

6.1. Sensitivity analysis. To better understand the main drivers of $\mathcal{R}_0$ and its sensitivity to parameter uncertainties, as it is a critical value in determining tumor eradication or escape, we utilize the PRCC method, where 1,000,000 Latin hypercube samples (LHSs) are taken for each parameter distribution. As there is uncertainty in parameter estimates, we assume a uniform distribution for all the ranges given in Table SM2 in the supplementary materials. For the parameters without ranges, we consider uniform distributions for ranges around 10^{-3} to 10^3 times the fixed values. In Figure 8a, we employ uniform sampling for all parameters. To avoid undersampling in intervals where the parameter values are very small, we use a log-uniform distribution, thus sampling on a logarithmic scale when the max/min $> 10^3$, with results shown in Figure 8b.

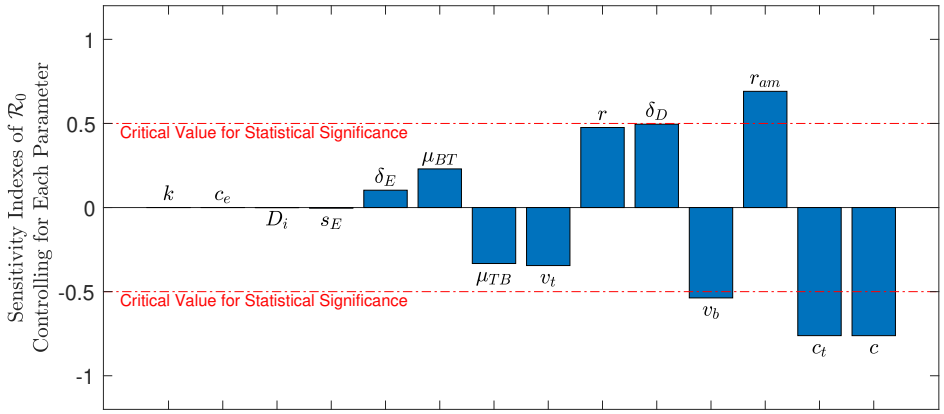

(a) Uniform sampling of parameter distributions

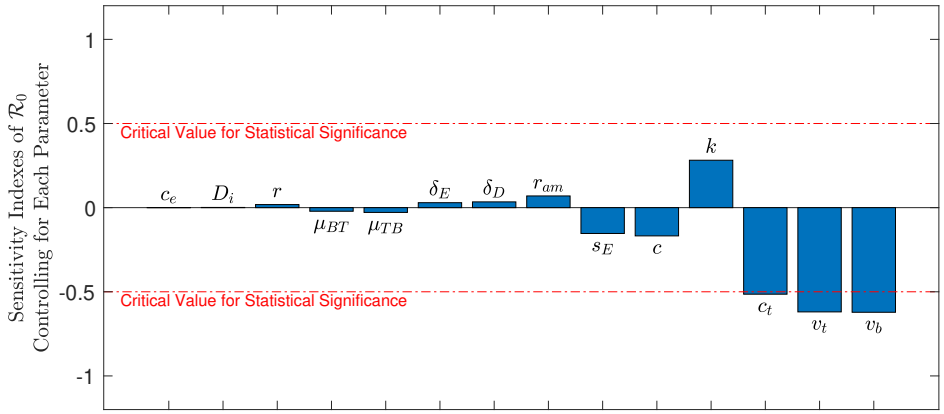

(b) Log-uniform sampling of parameter distributions (log scale if max/min $> 10^3$)

FIG. 8. *Sensitivity analysis is conducted using the PRCC method, where* 1,000,000 *LHSs are taken for each* (a) *uniform and* (b) *log-uniform parameter distribution. Combining results,* r_{am}, v_b, c_t, c, *and* v_t *are significant, where* r_{am} *is positively correlated with* $\mathcal{R}_0$.

The PRCC method reflects the correlation between $\mathcal{R}_0$ and parameters. PRCC values range from –1 to 1, where –1 indicates that the parameter is highly negatively correlated with $\mathcal{R}_0$, and 1 signifies that the parameter is highly positively correlated with $\mathcal{R}_0$. Figure 8a gives the principal parameters influencing $\mathcal{R}_0$ to be v_b, r_{am}, c_t, and c. The natural inactivation rate of CTLs (r_{am}) has the most significant positive effect on $\mathcal{R}_0$, while the intravenous dose amount (v_b), the kill rate of tumor cells by activated CTLs (c_t), and the activation/proliferation rate of CTLs (c) are similarly negatively correlated. The different methods of sampling lead to different results, as Figure 8b shows c_t, v_t, and v_b to be most significant, thus losing r_{am} and c and gaining v_t, the intratumoral dose amount. Combining results, r_{am}, v_b, c_t, c, and v_t are significant, where r_{am} is positively correlated with $\mathcal{R}_0$, and v_b, c_t, c, and v_t are negatively correlated.

Thus, for $\mathcal{R}_0$ to be low enough such that the tumor-free equilibrium is the only stable equilibrium, a high DC dosage amount, whether intravenous v_b or intratumoral v_t, or treatments targeting a decrease in r_{am} or an increase in c_t or c, would be most

effective. In particular, this suggests that a treatment to prolong the activation period for exhausted cells or to reactive exhausted effector cells, such as an immune checkpoint blockade, would be advantageous to combine with DC therapy. A rising interest in this combination over the last decade has led to the conception of various Phase I/II clinical trials researching a combined DC vaccine with an immune checkpoint blockade, with results still pending [45].

6.2. Dosing strategies. To consider a clinically relevant treatment, we consider a discrete treatment case by running simulations up to 600 days. We first standardize the time between injections while varying the dose amount, followed by standardizing the total dosage amount while varying the frequency of injection. Figure 9a displays the tumor cell response to various dose amounts given every 100 days over the course of 600 days, with DC doses ranging from 2×10^7 to 8×10^7 cells. Larger doses respond more positively, increasing the periods of tumor remission. With a large enough dose, tumor eradication is possible. Figure 9b depicts the amount of tumor cells when the total intravenous DC dose given over the 600 days is 4.5×10^8 with injections ranging from every day to every 150 days. If the entire dose is given on Day 1, without a follow-up treatment, the tumor aggressively grows to carrying capacity, as shown in Figure 9c.

Together our simulations suggest that larger, less frequent doses are more efficient in eradicating the tumor compared to the smaller, more frequent doses, though follow-up treatment is necessary to maintain control of the tumor. Unlike the majority of cancer treatments, toxicity has been determined to be a minimal issue for DC treatments, as flu-like symptoms are often the most adverse effect of DC vaccines. The low toxicity of DC vaccines allows higher, less frequent doses suggested by our model to be feasible in practice.

7. Discussion. We present a simple, autonomous, biologically meaningful mathematical model which accounts for observations found in the clinical setting. The reduced model is analytically tractable and admits rich dynamics. We have proven the existence of a backward bifurcation, given numerical evidence of a Hopf bifurcation, and given thresholds, C_9 and 1, for the combination parameter, $\mathcal{R}_0$, that guarantee the elimination ($\mathcal{R}_0 < C_9$) or existence ($\mathcal{R}_0 > 1$) of the tumor in the case of a continuous treatment. Since $\mathcal{R}_0$ decreases asymptotically to 0 as the treatment intensity (captured by v_b and v_t) increases, our model suggests that there is some level of treatment that will eradicate the tumor. Now $\mathcal{R}_0$ increases without bound with the proliferation rate of tumor cells. Therefore, our model suggests that if treatment is limited, aggressive cancers will continue to exist. In a subspace of the parameter space, the model exhibits bistability in the region $\mathcal{R}_{crit} < \mathcal{R}_0 < 1$. This suggests that more aggressive treatment strategies may be required than would be expected in the absence of the bistability.

As noted in Remark 5.1, there exists a double zero eigenvalue if we allow $\tilde{\delta}_E = 0$. This suggests the possibility of a BT bifurcation. The close proximity of pitchfork-like and Hopf bifurcations illustrated by numerical simulations and shown in Figure 4 provide further evidence of a possible BT bifurcation. It is known that a BT bifurcation may give rise to a homoclinic orbit. For our analysis, we assume that v_t and v_b are nonnegative and all other parameters are positive. Therefore, there is no BT in the relevant parameter space. Nevertheless, simulations suggest that system (2.2) admits a homoclinic orbit connecting the tumor-free equilibrium to itself. In the absence of this homoclinic connection, it is possible to show that the system

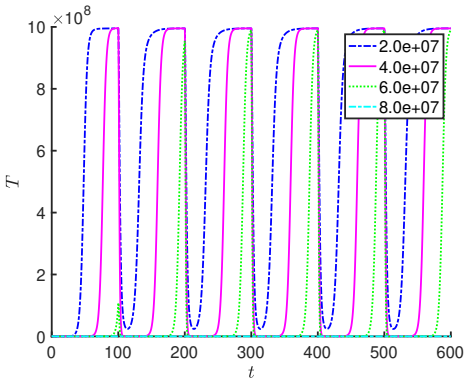

(a) Tumor with fixed timing, varying dose

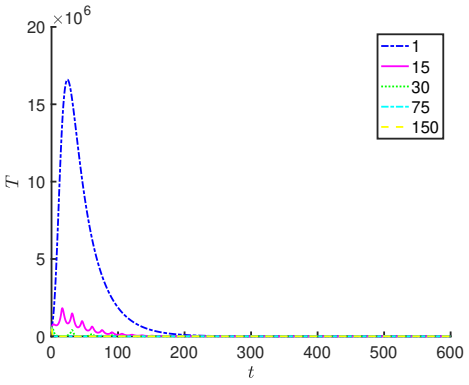

(b) Tumor with fixed dose, varying timing

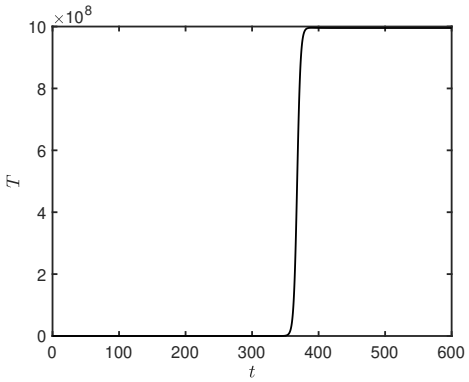

(c) Entire dose of 4.5×10^8 DCs on Day 1

FIG. 9. *Tumor response shown with respect to various doses and timings.* (a) *Intravenous injections of* 2×10^7 *to* 8×10^7 *cells given every* 100 *days for* 600 *days.* (b) *Total DC dose of* 4.5×10^8 *injected intravenously over* 600 *days, with injection times from every day to every* 150 *days.* (c) *Entire* 4.5×10^8 *DC dose injected intravenously on Day* 1.

is uniformly strongly persistent when $\mathcal{R}_0 > 1$. However, an analytic proof of the existence of this homoclinic connection and precise conditions for its existence remain open questions.

A sensitivity analysis using the PRCC method via LHSs reveals the main drivers of $\mathcal{R}_0$ that will most effectively lower $\mathcal{R}_0$, thereby improving the efficacy of the treatment. We conclude that the natural inactivation rate of CTLs (r_{am}) is most positively correlated with $\mathcal{R}_0$, while the intravenous dose amount (v_b), the intratumoral dose amount (v_t), the kill rate of tumor cells by activated CTLs (c_t), and the activation/proliferation rate of CTLs (c) are negatively correlated. An increased DC treatment, whether intratumoral or intravenous, in conjunction with a treatment targeting a decrease in r_{am} or an increase in c_t or c, would yield optimal results. Analysis regarding the critical subthreshold of $\mathcal{R}_0$, $\mathcal{R}_{\text{crit}}$, reveals that the tumor inactivation rate of CTLs (c_e) is important in the threshold sufficient for tumor eradication. Treatments to decrease c_e would similarly prove beneficial as a combination treatment. Immune checkpoint blockades would act to decrease r_{am}, and their combination with DC therapies is the subject of many ongoing clinical trials.

Acknowledgment. The authors would like to thank Dr. Craig J. Thalhauser for his valuable comments and help.

REFERENCES

[1] R. L. Siegel, K. D. Miller, and A. Jemal, *Cancer statistics,* 2019, CA: Cancer J. Clin., 69 (2019), pp. 7–34.
[2] V. W. Rebecca, V. K. Sondak, and K. S. M. Smalley, *A brief history of melanoma: From mummies to mutations*, Melanoma Res., 22 (2012), pp. 114–122.
[3] M. A. Wilson and L. M. Schuchter, *Chemotherapy for melanoma*, Cancer Treat. Res., 167 (2016), pp. 209–229.
[4] F. Castiglione and B. Piccoli, *Optimal control in a model of dendritic cell transfection cancer immunotherapy*, Bull. Math. Biol., 68 (2006), pp. 255–274.
[5] B. Domingues, J. M. Lopes, P. Soares, and H. Pópulo, *Melanoma treatment in review*, ImmunoTargets Ther., 7 (2018), pp. 35–49.
[6] A. Arabameri, D. Asemani, and J. Hajati, *Mathematical modeling of in-vivo tumor-immune interactions for the cancer immunotherapy using matured dendritic cells*, J. Biol. Systems, 26 (2018), pp. 167–188.
[7] J. Aerts and J. P. Hegmans, *Tumor-specific cytotoxic T cells are crucial for efficacy of immunomodulatory antibodies in patients with lung cancer*, Cancer Res., 73 (2013), pp. 2381–2388.
[8] F. O. Nestle, S. Alijagic, M. Gilliet, Y. Sun, S. Grabbe, R. Dummer, G. Burg, and D. Schadendorf, *Vaccination of melanoma patients with peptide- or tumorlysate-pulsed dendritic cells*, Nat. Med., 4 (1998), pp. 328–332.
[9] B. A. Tjoa, A.-A. A. Elgamal, and G. P. Murphy, *Vaccine therapy for prostate cancer*, Urol. Clin. North Am., 26 (1999), pp. 365–374.
[10] F. J. Hsu, C. Benike, F. Fagnoni, T. M. Liles, D. Czerwinski, B. Taidi, E. G. Engleman, and R. Levy, *Vaccination of patients with b-cell lymphoma using autologous antigen-pulsed dendritic cells*, Nat. Med., 2 (1996), pp. 52–58.
[11] U.S. National Library of Medicine, *ClinicalTrials.gov*, https://clinicaltrials.gov/.
[12] L. M. Liau, K. L. Black, N. A. Martin, S. N. Sykes, J. M. Bronstein, L. Jouben-Steele, P. S. Mischel, A. Belldegrun, and T. F. Cloughesy, *Treatment of a patient by vaccination with autologous dendritic cells pulsed with allogenic major histocompatibility complex class I-matched tumor peptides. Case report*, Neurosurg. Focus, 15 (2000), e8.
[13] D. Ridgway, *The first* 1000 *dendritic cell vaccinees*, Cancer Investig., 21 (2003), pp. 873–886.
[14] J. Wierecky, M. R. Müller, S. Wirths, E. Halder-Oehler, D. Dörfel, S. M. Schmidt, M. Häntschel, W. Brugger, S. Schröder, M. S. Horger, L. Kanz, and P. Brossart, *Immunologic and clinical responses after vaccinations with peptide-pulsed dendritic cells in metastatic renal cancer patients*, Cancer Res., 66 (2006), pp. 5910–5918.
[15] L. Fong, Y. Hou, A. Rivas, C. Benike, A. Yuen, G. A. Fisher, M. M. Davis, and E. G. Engleman, *Altered peptide ligand vaccination with Flt3 ligand expanded dendritic cells for tumor immunotherapy*, Proc. Natl. Acad. Sci. USA, 98 (2001), pp. 8809–8814.
[16] A. Ferrara, M. Nonn, P. Sehr, C. Schreckenberger, M. Pawlita, M. Dürst, A. Schneider, and A. M. Kaufmann, *Dendritic cell-based tumor vaccine for cervical cancer* II: *Results of a clinical pilot study in* 15 *individual patients*, J. Cancer Res. Clin. Oncol., 129 (2003), pp. 521–530.
[17] O. Markov, N. Mironova, S. Sennikov, V. Vlassov, and M. Zenkova, *Prophylactic dendritic cell-based vaccines efficiently inhibit metastases in murine metastatic melanoma*, PLoS One, 10 (2015), e0136911.
[18] M. van Gulijk, F. Dammeijer, J. G. J. V. Aerts, and H. Vroman, *Combination strategies to optimize efficacy of dendritic cell-based immunotherapy*, Front. Immunol., 9 (2018), 2759.
[19] T. Burden, J. Ernstberger, and K. R. Fister, *Optimal control applied to immunotherapy*, Discrete Contin. Dyn. Syst. Ser. B, 4 (2004), pp. 135–146.
[20] A. Cappuccio, F. Castiglione, and B. Piccoli, *Determination of the optimal therapeutic protocols in cancer immunotherapy*, Math. Biosci., 209 (2007), pp. 1–13.
[21] L. G. de Pillis, W. Gu, K. R. Fister, T. Head, K. Maples, A. Murugan, T. Neal, and K. Yoshida, *Chemotherapy for tumors: An analysis of the dynamics and a study of quadratic and linear optimal controls*, Math. Biosci., 209 (2007), pp. 292–315.
[22] A. Ghaffari and N. Naserifar, *Optimal therapeutic protocols in cancer immunotherapy*, Comput. Biol. Med., 40 (2010), pp. 261–270.
[23] J. L. Gevertz and J. R. Wares, *Developing a minimally structured mathematical model*

of cancer treatment with oncolytic viruses and dendritic cell injections, Comput. Math. Methods Med., 2018 (2018), 8760371, https://doi.org/10.1155/2018/8760371.

[24] E. Castillo-Montiel, J. C. Chimal-Eguía, J. I. Tello, G. Piñon-Zaráte, M. Herrera-Enríquez, and A. E. Castell-Rodríguez, *Enhancing dendritic cell immunotherapy for melanoma using a simple mathematical model*, Theor. Biol. Med. Model., 12 (2015), 11.

[25] L. de Pillis, A. Gallegos, and A. Radunskaya, *A model of dendritic cell therapy for melanoma*, Front. Oncol., 3 (2013), 56.

[26] B. Ludewig, P. Krebs, T. Junt, H. Metters, N. J. Ford, R. M. Anderson, and G. Bocharov, *Determining control parameters for dendritic cell-cytotoxic t lymphocyte interactions*, Eur. J. Immunol., 34 (2004), pp. 2407–2418.

[27] T. H. Lee, Y. H. Cho, and M. G. Lee, *Larger numbers of immature dendritic cells augment an anti-tumor effect against established murine melanoma cells*, Biotechnol. Lett., 29 (2007), pp. 351–357.

[28] D. Kirschner and J. C. Panetta, *Modeling immunotherapy of the tumor-immune interaction*, J. Math. Biol., 37 (1998), pp. 235–252.

[29] M. Berard and D. F. Tough, *Qualitative differences between naive and memory T cells*, Immunology, 106 (2002), pp. 127–138.

[30] E. Nikolopoulou, L. R. Johnson, D. Harris, J. D. Nagy, E. C. Stites, and Y. Kuang, *Tumour-immune dynamics with an immune checkpoint inhibitor*, Lett. Biomath., 5 (2018), pp. S137–S159.

[31] T. Portz and Y. Kuang, *A mathematical model for the immunotherapy of advanced prostate cancer*, in BIOMAT 2012, R. P. Mondaini, ed., World Scientific, Singapore, 2013, pp. 70–85.

[32] L. A. Dethlefsen, J. M. S. Prewitt, and M. L. Mendelsohn, *Analysis of tumor growth curves*, J. Natl. Cancer Inst., 40 (1968), pp. 389–405.

[33] L. Norton, *A Gompertzian model of human breast cancer growth*, Cancer Res., 48 (1988), pp. 7067–7071.

[34] L. Polo-Parada, G. Gutiérrez-Juárez, D. Cywiak, R. Pérez-Solano, and G. A. Baker, *Spectrophotometric analysis at the single-cell level: Elucidating dispersity within melanic immortalized cell populations*, Analyst, 142 (2017), pp. 1482–1491.

[35] D. F. Tough and J. Sprent, *Turnover of naive- and memory-phenotype t cells*, J. Exp. Med., 179 (1994), pp. 1127–1135.

[36] C. A. Michie, A. McLean, C. Alcock, and P. C. L. Beverley, *Lifespan of human lymphocyte subsets defined by CD45 isoforms*, Nature, 360 (1992), pp. 264–265.

[37] J. M. McCune, M. B. Hanley, D. Cesar, R. Halvorsen, R. Hoh, D. Schmidt, E. Wieder, S. Deeks, S. Siler, R. Neese, and M. Hellerstein, *Factors influencing T-cell turnover in HIV-1-seropositive patients*, J. Clin. Investig., 105 (2000), pp. R1–R8.

[38] O. Diekmann, J. A. P. Heesterbeek, and J. A. J. Metz, *On the definition and computation of the basic reproduction ratio R_0 in models for infectious diseases in heterogeneous populations*, J. Math. Biol., 28 (1990), pp. 365–382.

[39] P. van den Driessche and J. Watmough, *Reproduction numbers and sub-threshold endemic equilibria for compartmental models of disease transmission*, Math. Biosci., 180 (2002), pp. 29–48.

[40] H. L. Smith, *Monotone dynamical systems: An introduction to the theory of competitive and cooperative systems*, Math. Surveys Monogr. 41, American Mathematical Society, Providence, RI, 1995.

[41] C. Castillo-Chavez and B. Song, *Dynamical models of tuberculosis and their applications*, Math. Biosci. Eng., 1 (2004), pp. 361–404.

[42] A. B. Gumel, *Causes of backward bifurcations in some epidemiological models*, J. Math. Anal. Appl., 395 (2012), pp. 355–365.

[43] K. F. Bol, E. H. Aarntzen, F. E. Hout, G. Schreibelt, J. H. Creemers, W. J. Lesterhuis, W. R. Gerritsen, D. J. Grunhagen, C. Verhoef, C. J. Punt, J. J. Bonenkamp, J. H. de Wilt, C. G. Figdor, and I. J. de Vries, *Favorable overall survival in stage* III *melanoma patients after adjuvant dendritic cell vaccination*, Oncoimmunology, 5 (2016), e1057673.

[44] Y. A. Kuznetsov, *Elements of Applied Bifurcation Theory*, 2nd ed., Springer, New York, 1998.

[45] M. Versteven, J. M. J. Van den Bergh, E. Marcq, E. L. J. Smits, V. F. I. Van Tendeloo, W. Hobo, and E. Lion, *Dendritic cells and programmed death-1 blockade: A joint venture to combat cancer*, Front. Immunol., 9 (2018), 394.